Title
Transition-metal redox evolution in LiNi0.5Mn0.3Co0.2O2 electrodes at high potentials

Authors
Qiao, Ruimin
Liu, Jun
Kourtakis, Kostantinos
et al.

Publication Date
2017-08-01

DOI
10.1016/j.jpowsour.2017.06.009

Peer reviewed

Transition-Metal Redox Evolution in $LiNi_{0.5}Mn_{0.3}Co_{0.2}O_2$ Electrodes at High Potentials

Ruimin Qiao[a], Jun Liu[b§], Kostantinos Kourtakis[b], Mark G. Roelofs[b§], Darin L. Peterson[b§], James P. Duff[b§], Dean T. Deibler[b§], Andrew Wray[c], Wanli Yang[a]**

[a] Advanced Light Source, Lawrence Berkeley National Laboratory, Berkeley, CA 94720

[b] DuPont Company, Experimental Station, Wilmington, DE, 19803

[c] Department of Physics, New York University, New York, NY 10003

[§] Currently not affiliated with DuPont

ABSTRACT

The mixed transition-metal layered compound, $LiNi_{0.5}Mn_{0.3}Co_{0.2}O_2$ (NMC532), is a promising high-energy cathode material. However, the required high-voltage (>4.3 V) cycling is accompanied by a rapid capacity fade associated with a complex redox mechanism that has not been clarified. Here we report soft x-ray absorption spectroscopy of NMC532 electrodes, both pristine and those charged to 4.2, 4.35, or 4.5 V in graphite/NMC532 cells. A quantitative sXAS analysis shows that about 20% of the nickel exists as Ni^{4+} in the as-synthesized NMC532. The experimental capacity of NMC532 electrodes obtained below 4.2 V is from the redox of both Ni and Co. However, Co redox reactions take place throughout the electrochemical cycling and are the only observed transition-metal redox reactions above 4.2 V. In contrast to the changing ratio of the well-defined Ni^{2+}, Ni^{3+} and Ni^{4+} ions, Co always displays ill-defined intermediate valence states in the charged NMC532 electrodes. This indicates an itinerant electron system in NMC electrodes related to the improved rate performance through Co doping. Additionally, about 20% of Ni^{2+} is found on the electrode surface at the high potential, which suggests that the electrode surface has either gone through surface reconstruction or reacted with the electrolyte at high voltage.

KEYWORDS: lithium-ion batteries, $LiNi_{0.5}Mn_{0.3}Co_{0.2}O_2$, high voltage, soft x-ray spectroscopy.

Introduction

With growing global concerns about environmental deterioration and climate change, there is an urgent need to explore renewable energy sources and to develop efficient energy storage systems. Lithium-ion batteries (LIBs), which are known for their applications in portable electronics and now electric vehicles, have the highest energy density among all widely adopted energy storage techniques[1, 2]. Extensive efforts have therefore been made to further improve the electrochemical performance of LIBs, and especially to search for high capacity cathode materials. Layered lithium transition metal (TM) oxides, which have the α-$NaFeO_2$ structure and the general chemical formula, $LiNi_xMn_yCo_zO_2$ (NMC) (x+y+z=1), are cathode materials that are currently under extensive studies with the high theoretical capacity of about 280 mAh g^{-1} [3-10]. In this family, $LiCoO_2$ was the one adopted in the first commercial LIBs in 1990, although only about half of its theoretical capacity was utilized due to the cycling instability [11].Later on, Ni and Mn ions were introduced into the system in attempts to improve the performance and to reduce the cost. In recent years, $LiNi_{1/3}Mn_{1/3}Co_{1/3}O_2$ (NMC111) and $LiNi_{0.5}Mn_{0.3}Co_{0.2}O_2$ (NMC532) are also commercially adopted in Li-ion battery products. However, despite of extensive efforts made by researchers, the practical capacities of these materials are still limited because high voltage operation (>4.3V) required for the high capacity is accompanied by a rapid capacity fade.

It is generally believed that the lithium insertion/extraction, which is accompanied by changes in the chemical valence and electronic structure of the transition metal elements, could cause structural instability of the electrode and/or side reactions at the electrode-electrolyte interface. Electronic and crystal structures are both fundamental to the electrochemical performance of the material. Based on numerous electrochemical data, the empirical rules about various NMC electrode materials with different compositions are that Ni contributes to the high capacity at the expense of safety characteristics; Co improves the rate performance at the expense of cost, and Mn enhances the structural stability at the expense of capacity[12, 13]. To address the different roles each TM elements play in the electrochemical performance of the NMC materials, it is important to have a deeper understanding of the evolving electronic structures of these TM ions.

Although many studies have been done to address the structural transformation of NMC electrodes [8, 12, 14], there are only a few reports on the evolving transition metal electronic structure. Previously, temperature-dependent magnetization measurement[15] , x-ray photoelectron spectroscopy (XPS)[9], electron energy loss spectroscopy (EELS) [16], TM *K*-edge hard x-ray absorption spectroscopy (XAS)[5, 17-21] and *L*-edge soft x-ray absorption spectroscopy (sXAS) have been applied for studying the transition metal electronic structure in various battery materials. In particular, Yoon et. al reported the TM *K*-edge XAS results of NMC111, which shows that the major charge compensation during lithium deintercalation is achieved by the oxidation of Ni^{2+} ions, while the other two transition metal elements remain mostly unchanged in the Mn^{4+} and Co^{3+} states[5]. For the same material, Kim et. al found that the oxidation reaction of Ni^{2+}/Ni^{4+} is related to the lower plateau around 3.75V, but that of Co^{3+}/Co^{4+} seems to occur in the entire range of charging up to 4.7V[21]. We would like to point out that although hard x-rays benefit from deep penetration depth and non-vacuum instrumentation, the dominating signal of TM *K*-edge XAS is from the *4p* states, which are not the valence state of transition metals. The TM-*3d* valence states only exhibit weak features through the low intensity dipole-forbidden quadrupole *s-d* transitions. On the other hand, TM *L*-edge sXAS probes directly the *3d* unoccupied valence states of TM through the dipole *2p-3d* transitions. Therefore, it can reveal abundant information about the TM 3*d* electrons. The quantitative analysis of the TM oxidation states is only enabled by the high-resolution TM *L*-edge sXAS[17, 22-28]. Moreover, it has both surface and bulk sensitivities and therefore is able to provide contrast between electrode surface and bulk [25, 29, 30].

In this work, we study the evolving transition metal electronic structure in pristine and charged NMC532 electrodes with the cutoff voltages up to 4.5 V using synchrotron-based soft x-ray absorption spectroscopy (sXAS). We provide direct spectral evidence that the experimental capacity of NMC532 obtained below 4.2 V is related to both Ni and Co redox reactions, while only Co redox reactions are observed above 4.2 V. Furthermore, unlike the well-defined Ni redox and valences, Co displays ill-defined intermediate states throughout the electrochemical charging process, indicating a delocalized electron system promoted by Co, as in the case of $LiCoO_2$. This

is related with the improved rate performance through Co doping in the material. In addition, about 20% of Ni^{2+} is observed on the electrode surface at 4.5 V, which indicates the electrode surface has either gone through surface reconstruction or reacted with the electrolyte at high voltage.

Experimental Section

1. Material synthesis, structural and electrochemical characterization

Powder X-ray diffraction (XRD) measurements of pristine NMC532 powder (Jinhe, China) were carried out with a Philips X'PERT (Model 3040) using Cu-*K*α radiation between 4-80 degrees with a scan rate of 0.015 degree/s. The NMC532 powder, carbon black, and PVDF were thoroughly mixed in N-Methyl-2-pyrrolidone (NMP) solvent in a weight ratio of 90:5:5, to form a cathode paste. The cathode paste was coated on Al foil via a doctor blade method, followed by a thorough drying step. The as-made NMC532 cathode, along with a graphite (Gr) anode, and Celgard® 2500 separator, were used to assemble pouch cells. Suitable amounts of ethylene carbonate (EC) / ethyl methyl carbonate (EMC) (30/70 weight ratio) with 1 M $LiPF_6$ electrolyte (purchased from BASF) were injected into the pouch cells before sealing. After formation, the Gr/NMC532 pouch cells were charged to various voltages (i.e., 4.2 V, 4.35 V, or 4.5 V), immediately followed by a careful disassembly of the cells in an argon filled glove box. The charged NMC532 cathodes were rinsed with dimethyl carbonate (DMC) solvent and dried in the glove box. These cathode samples were then loaded into the ultra-high vacuum sXAS characterization chamber through a sample transfer kit to avoid any air exposure.

2. sXAS experiments and calculations

sXAS was performed at Beamline 8.0.1 of the Advanced Light Source (ALS) in Lawrence Berkeley National Lab (LBNL). The undulator and spherical grating monochromator supply a linearly polarized photon beam with resolving power up to 6000. The experimental energy resolution is about 0.15 eV. Experiments were performed at room temperature and with the linear polarization of the incident beam oriented at 45° to the sample surfaces. The sXAS spectra were collected using both total electron yield (TEY), with a probing depth around 10 nm, and

total fluorescence yield (TFY) with a probing depth larger than 100 nm. All the spectra have been normalized to the beam flux measured by the upstream gold mesh.

Calculations were performed for a single impurity Anderson model (SIAM), describing the 2*p* and 3*d* orbitals of Ni and a 3 eV wide ligand band that can contain up to one hole. Implementation follows the treatment in Ref.[31]. Slater-Condon parameters were renormalized to 80%, 75% and 70% of Hartree-Fock values for nominal Ni^{2+}, Ni^{3+} and Ni^{4+} calculations, respectively, and the initial state ensemble was Boltzmann weighted to T=300K. The crystal field is given by 10Dq= 0.5, 2.0, and 2.5, in ascending order for higher valence, and metal-ligand hopping is assigned a similar trend with V_{eg}=2, 2.5 and 3 eV. The t_{2g} symmetry hopping parameter is assigned half the amplitude of e_g hopping (V_{t2g}=-V_{eg}/2). Configuration energies with a ligand hole were set to $E(d^{n+1})$-$E(d^n)$=3.5, 0.5, and -2 eV without a core hole and $E(d^{n+1})$-$E(d^n)$=3.1, -0.9, and -4.4 with a core hole present, for ascending valence. These parameters yield a high spin state for Ni^{2+}, and low spin states for Ni^{3+} and Ni^{4+}, and are similar to parameter sets in Ref. [31, 32]. Simulations of TEY are obtained by calculating the cross section for dipole transitions from the initial thermal ground state ensemble to the core hole states. The TFY simulations include an additional matrix element for photon emission in the detector direction, described by the Kramers-Heisenberg equation.

Results and Discussion

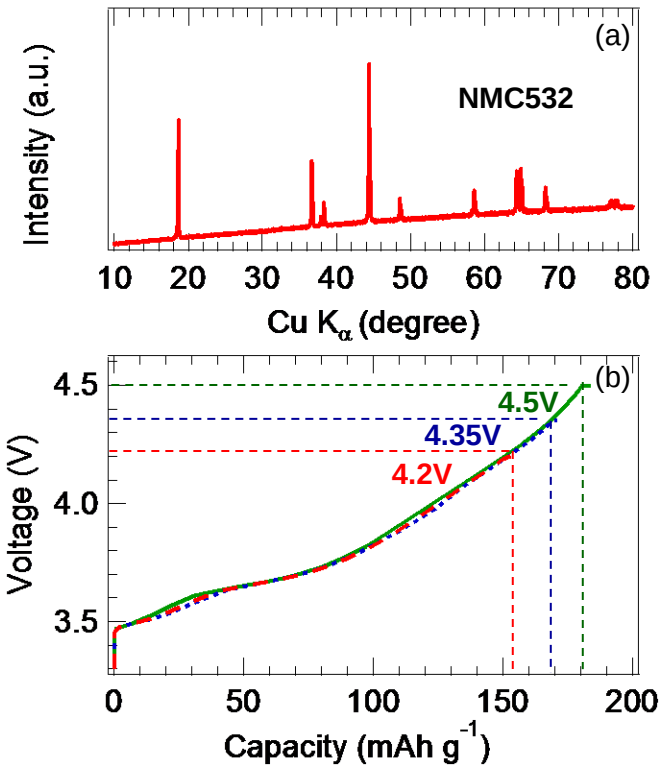

Figure 1. (a) XRD of the pristine NMC532 powder. (b) Charge curves of Gr/NMC532 cells when they are charged to 4.2 V, 4.35 V, or 4.5 V, respectively.

The XRD pattern of the NMC532 powder is shown in Fig. 1 (a), which indicates that the cathode powder has the typical layered structure of a hexagonal α-$NaFeO_2$ type with a space group of R3m (no. 166)[33]. After formation, the graphite/NMC532 pouch cells were charged at a constant current of 0.2C to various cutoff voltages (vs. the graphite anode), followed by a constant voltage charge until the current decayed to 0.05C. The charge curves with various cutoff charge voltages are shown in Fig. 1 (b). The charge capacity at 4.2 V was 154 mAh g^{-1} and the increase was ~12% when elevating the charge cutoff voltage from 4.2 to 4.35 V, while the capacity increase was an additional ~8% when further increasing the charge cutoff voltage from 4.35 to 4.5 V. The other interesting observation was that the "tail" (capacity obtained in the constant voltage charge step) becomes longer when increasing the charge cutoff voltages. This could be associated with an impedance growth caused by a cathode interfacial side reaction with electrolyte at higher voltage [10, 34].

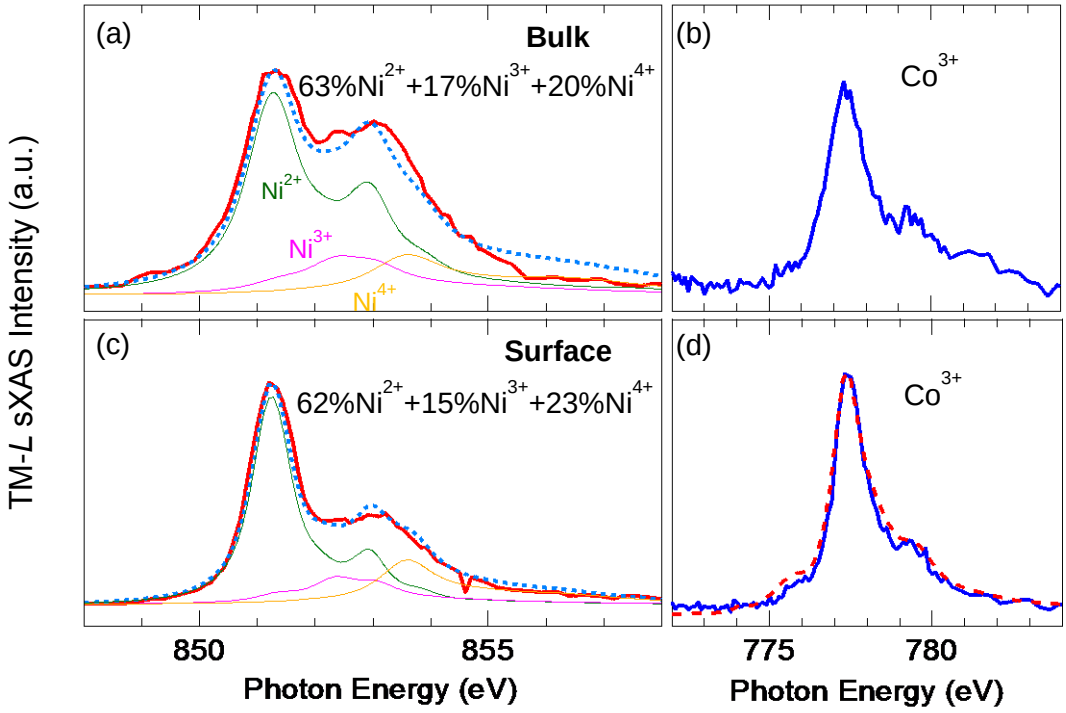

Figure 2. Ni (a, c) and Co (b, d) L_3-edge sXAS spectra of pristine NMC532. Both bulk-sensitive TFY sXAS spectra with the probing depth of around 100nm (top panels) and surface-sensitive TEY with the probing-depth of less than 10nm (bottom panels) are shown. For Ni (a and c), the simulated sXAS spectra using the linear combination of Ni^{2+}, Ni^{3+} and Ni^{4+} reference spectra are shown in the blue dashed lines, which agree well with the experimental spectra (red solid lines). The fitting analyzes the Ni^{2+}, Ni^{3+} and Ni^{4+} concentration in pristine NMC532. Note that the different spectral lineshapes of the surface and bulk signals are due to the different detection channels, which is accounted for in the calculated reference spectra. Meanwhile, only Co^{3+} (b and d) are observed in the pristine samples. The dashed line in (d) is from the reference sample $LiCoO_2$[25].

In order to determine the initial oxidation states of all three transition metal elements in the pristine NMC532, sXAS studies were carried out at the Ni, Mn and Co *L*-edges (Fig. 2 and Fig. S1). The transition metal *L*-edge sXAS spectra can be divided into two regions, the L_3-edge at lower photon energy and the L_2-edge at higher energy, due to 2p core hole spin−orbital splitting. In general, the L_2-edge displays much broader absorption features than the L_3-edge due to shorter lifetime of the $2p_{1/2}$ core hole as a consequence of Coster-Kronig Auger decay[35, 36]. Therefore, in this paper we will mainly focus on the analysis of the L_3-edge absorption profile.

We have previously demonstrated that transition metal oxides show dramatically different sXAS profiles, which enables reliable quantitatively analysis of the TM oxidation states in battery electrodes [25-27, 37, 38]. Moreover, both bulk-sensitive and surface-sensitive information could be obtained simultaneously through different detection modes, TFY and TEY, respectively. TFY is a photon-in photon-out technique with the probing depth of around 100nm while TEY is photon-in electron-out and has the probing depth of less than 10nm due to the strong interaction of electrons with the matter [39].

For Ni (Fig. 2a and 2c), the experimental spectra are shown in red thick lines, and the simulated spectra using the linear combination of Ni^{2+}, Ni^{3+} and Ni^{4+} reference are plotted in blue dashed lines. The Ni^{2+}, Ni^{3+} and Ni^{4+} reference spectra are calculated in octahedral crystal field using the single impurity Anderson model. Note that the TFY spectra are slightly different from TEY, especially for Ni^{2+}, which is due to the self-absorption effects of TFY that tend to suppress the high intensity peak[39]. It is evident, by simply comparing with the three reference spectra, that nickel in pristine NMC532 has mixed oxidation states. The simulated spectra agree well with the experimental data. The associated fitting results show that the electrode bulk is composed of 63% Ni^{2+}, 17% Ni^{3+} and 20% Ni^{4+}, and it is consistent with the Ni concentration on the electrode surface (62% Ni^{2+},15% Ni^{3+} and 23% Ni^{4+}) within a reasonable error range.

The finding of about 20% of Ni^{4+} in the pristine NMC532 electrode is very surprising but meaningful. Empirically, one would expect there are 60% Ni^{2+}, 40% Ni^{3+} and 0% Ni^{4+} in stoichiometric NMC532 as Mn takes the 4+ oxidation state and Co is 3+. To increase electrochemical performance, NMC materials are often produced with Li:TM ratios slightly above 1.00, e.g. $Li_1(Li_{0.04}(Ni_{0.5}Mn_{0.3}Co_{0.2})_{0.96})O_2$. Here Li^+ is present in the TM layer, TM:O drops below 1:2, and the TM elements need higher oxidation states to balance the oxide ions. Moreover, our Mn and Co data indeed shows that only Mn^{4+} (Fig. S1) and Co^{3+} (Fig. 2b and 2d) are found in the pristine NMC532.

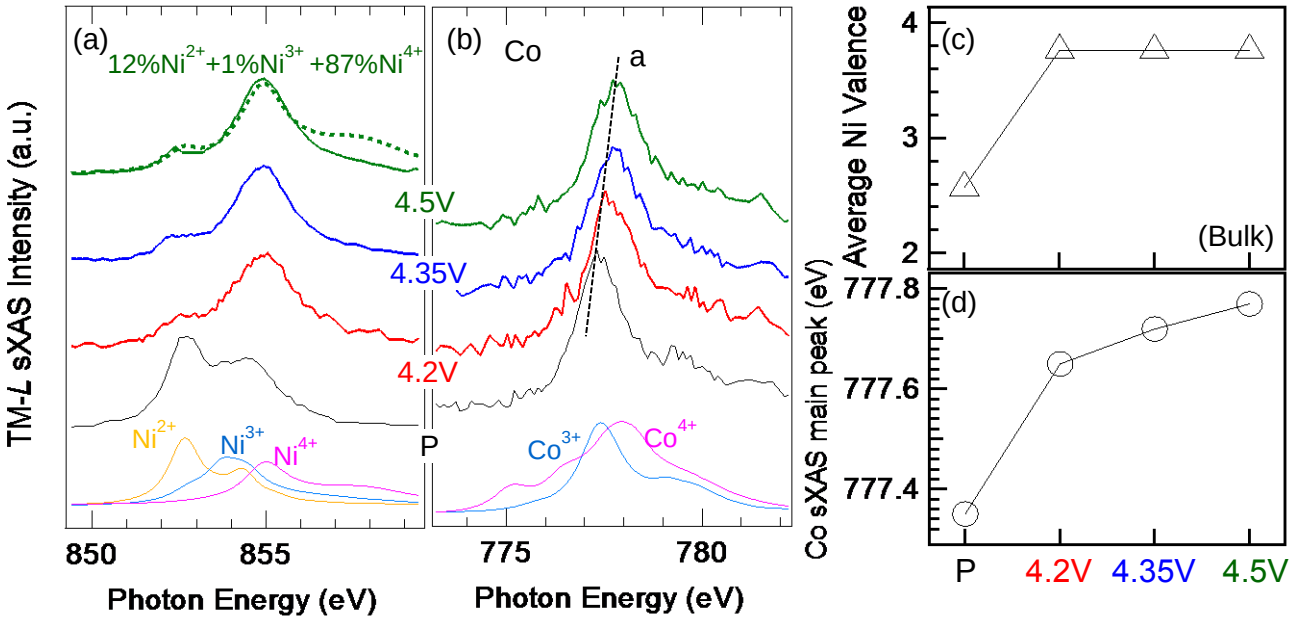

Figure 3. Evolution of the Ni and Co oxidation states in the bulk of the NMC532 electrode as a function of the charging voltage revealed by Ni-L_3 (a) and Co-L_3 (b) sXAS spectra collected in TFY mode. In (a) and (b), the calculated TFY sXAS spectra with the defined oxidation states in an octahedral crystal field are shown at the bottom, and the experimental spectra collected on NMC532 electrodes at different voltages are shown on top. The dashed line in (a) is the simulated spectrum which reveals the relative Ni^{2+}, Ni^{3+} and Ni^{4+} concentrations in the charged electrodes. (c) The calculated average Ni oxidation state, derived from sXAS spectra, as a function of the charging voltage. (d) The energy position of the Co sXAS main peak as a function of the charging voltage.

The electrochemical cycling process of NMC532 is essentially a redox reaction with evolving oxidation states of its constituent elements, which are tracked by sXAS spectra of all three TM *L*-edges and the oxygen *K*-edge. Both bulk-sensitive TFY and surface-sensitive TEY spectra are collected to provide depth-dependent information. Fig. 3 (a) and (b) show the bulk-sensitive Ni and Co L_3-edge TFY sXAS spectra, with their full range *L*-edge spectra displayed in Figs. S2 – S3. The Mn *L*-edge sXAS spectra are displayed in Fig. S1, which stay unchanged at different voltages. This is consistent with the common belief that Mn^{4+} is electrochemically inactive in NMC532.

In Fig. 3 (a), the Ni spectral lineshape changes dramatically when the electrode is charged to 4.2 V, but then remains the same with further potential increase. This provides direct evidence that Ni redox only contributes to the capacity of the NMC532 electrodes below 4.2 V. The quantitative fitting results reveal that there are 12% of Ni^{2+}, 1% of Ni^{3+} and 87% of Ni^{4+} in the charged electrodes. As compared with the pristine electrode (Fig. 2), the majority of Ni^{2+} and Ni^{3+} turn into Ni^{4+} when the NMC532 electrode is charged to 4.2 V. The amount of remaining Ni^{3+} in the charged electrode is negligible. However, there is still 12% of Ni^{2+} left in the charged sample. In fact, the electrochemically inactive Ni^{2+} has been observed in many Ni-based electrode materials, especially on the electrode surface. Both surface reconstruction and reactions with the electrolyte during high voltage operation could lead to the formation of the electrochemically inactive Ni^{2+} compounds [13, 27, 40]. The direct evidence of such surface Ni^{2+} is elaborated later in this manuscript.

Cobalt also plays an important role in the electrochemical reaction of NMC532 as evidenced by its spectral evolution (Fig. 3(b)). Unlike Ni, the overall lineshape of Co-L_3 sXAS does not change much, however, its main sXAS peak gradually shifts towards higher energy upon the increasing voltage, which suggests the $Co^{3+/4+}$ redox. The energy position of the Co-L_3 sXAS main peak as a function of the charging voltage is displayed in Fig. 3(d). Although the majority of the charge capacity and the strongest energy shift takes place below 4.2 V, the gradually shifting sXAS peak position is clear in both the peak position plot in Fig. 3(d) and the raw data in Fig. 3(b), indicating that the Co oxidation state keeps increasing with the voltage up to 4.5 V. Therefore, throughout the charging process, the Co contributes to the capacity of the NMC532 electrodes, and Co redox is the only TM redox contributing to the high-voltage capacity from 4.2 V to 4.5 V.

We would like to point out that, although the peak shifts are indicative of Co oxidation states increasing from Co^{3+} towards Co^{4+}, in contrast to the case of Ni, a linear combination of Co^{3+} and Co^{4+} reference spectra could never fit the experimental spectra well. This implies that the Co states in the charged NMC532 electrodes do not simply consist of well-defined Co^{3+} and Co^{4+}. Instead, the Co sXAS shows an averaged intermediate oxidation states in the electrode, indicating an itinerant electron system, especially on the lowest energy Co 3*d* a_{1g} orbital, with strong electronic correlation and polaronic effects as in $LiCoO_2$ [41]. We note that such an

itinerant electron system fundamentally improves the overall electric conductivity by delocalizing the charges, which could be the fundamental mechanism of the improved rate performance through Co doping in NMC systems.

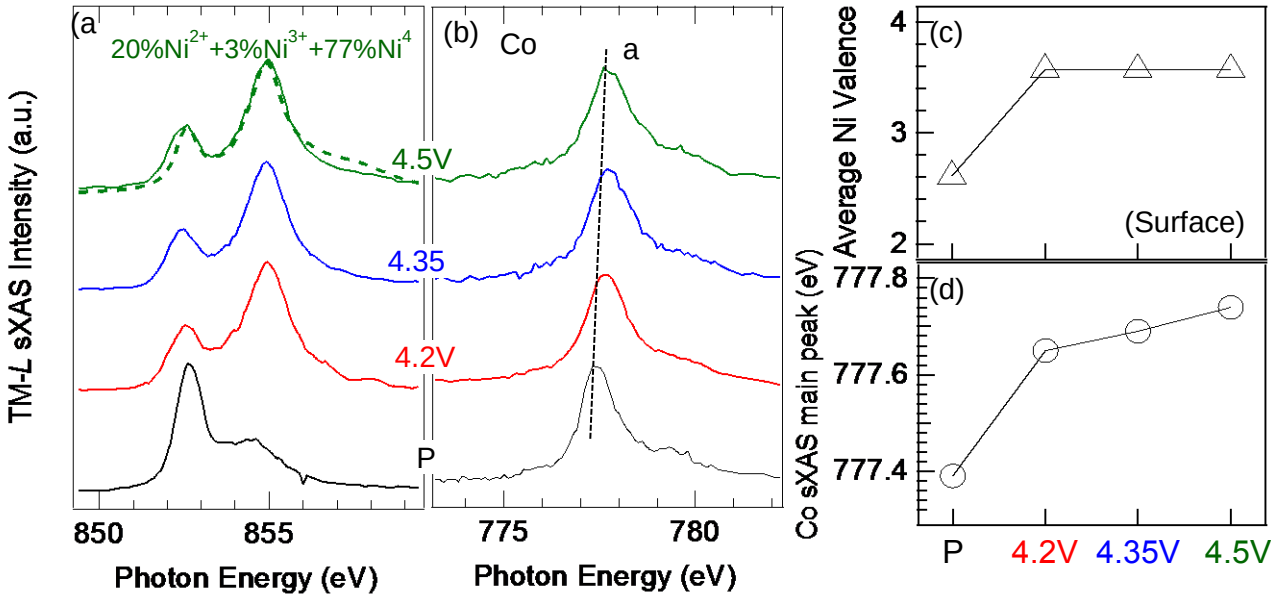

Figure 4. Evolution of the Ni and Co oxidation states on the NMC532 electrode surface as a function of the charging voltage revealed by Ni-L_3 (a) and Co-L_3 (b) sXAS spectra collected in the TEY mode. The dashed line in (a) is the simulated spectrum which reveals the ratio of Ni^{2+}, Ni^{3+} and Ni^{4+} concentration on the charged electrode surface. (c) The calculated average Ni oxidation state through sXAS spectra as a function of the charging voltage. (d) The energy position of the Co sXAS main peak as a function of the charging voltage.

In order to elucidate the surface behavior of the NMC electrodes at high voltages, as briefly mentioned above, Fig. 4 shows the surface-sensitive Ni and Co L_3-edge TEY sXAS spectra as a function of the charging voltage. Again, the Mn L-edge TEY spectra are displayed in Fig. S1(b), which show unchanged Mn^{4+} in all the samples. Although sXAS using high-intensity synchrotron light is sensitive to even a small quantity of Mn^{2+} ions on the electrode surface [27, 38], no Mn^{2+} was detected on the NMC532 electrode surface, suggesting that the Mn^{4+} ions in NMC532 are very stable against electrochemical cycling. As Mn^{2+} is notorious for its close relation with transition metal dissolution[3, 27, 42, 43], the absence of Mn^{2+} on NMC532 electrode surface suggests that the main cause of NMC532 degradation is likely not related to

Mn dissolution[13]. Both the Ni and Co L_3-edge TEY sXAS spectra display similar overall behavior with voltage as that of the bulk TFY data (Fig. 3). However, the Ni^{2+} concentration from the TEY and TFY signals is dramatically different on the charged electrodes. Despite that the Ni valence concentration of the pristine NMC electrode is the same for the bulk and surface, the charged electrodes have 20% of Ni^{2+} on the surface compare with 12% in the bulk. Considering the bulk signal also includes the contribution from the surface, the results indicate that majority of the inactive Ni^{2+} concentrates on the surface of the electrodes. This may arise from the surface reconstruction and/or reactions with the electrolyte during high voltage operation [12, 27, 44-46].

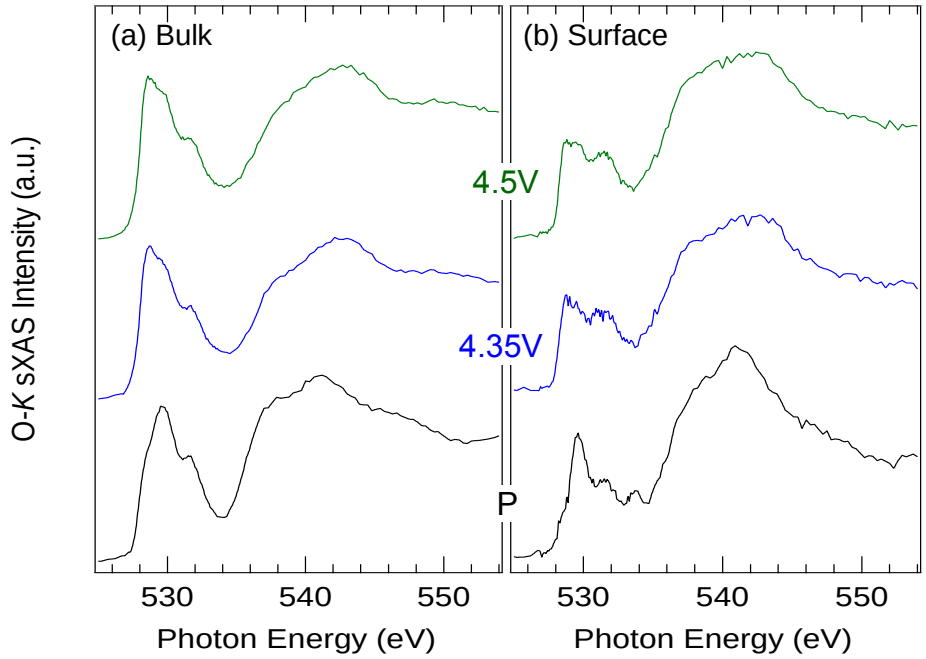

Figure 5. Evolution of the O *K*-edge sXAS spectra of the NMC532 electrodes at different voltage. Both bulk-sensitive TFY (a) and surface-sensitive TEY spectra (b) are shown.

Fig. 5 shows the bulk-sensitive and surface-sensitive O *K*-edge sXAS spectra of the NMC532 electrodes at different voltage. O *K*-edge sXAS spectra originate from electron dipole transitions between O 1*s* and 2*p* orbitals. The absorption features can be roughly divided into two groups, i.e., the pre-edge region (527-534 eV) with sharp peaks, which is mainly from the hybridization between O-2*p* and localized TM-3*d* orbitals, and the broad peak region (above 534 eV), which is associated with the O-2*p* hybridized with the itinerant valence electron orbitals of the ions that

are bonded to the oxygen [47]. The bulk-sensitive O-*K* TFY sXAS spectra (Fig. 5 (a)) exhibit clear voltage-dependent spectral evolution in the pre-edge region (527-534 eV), which reflects the cycling behavior of the transition metal ions in the bulk NMC532 electrode. When the electrodes are charged at high voltage, electrons are removed from the TM-3*d* orbitals. The increased low-energy absorption intensity at around 529eV is related to the increased TM-3*d* holes [26]. The contrast between the surface-sensitive TEY signal (Fig. 5a) and bulk-sensitive TFY signal (Fig.5b) is due to the oxygen-containing decomposition products of the electrolyte, which suppress the O-2*p* and TM-3*d* hybridization features from the electrode[30]. In general, the overall lineshape change of the O *K*-edge sXAS spectra at the pre-edge regime is consistent with the TM *L*-edge results and with other Ni redox systems[26]. We have to note that recent reports on layered battery compounds suggest possible oxygen redox at high potentials [48-50], and changes on O-*K* sXAS in the pre-edge range have also been discussed in Li-rich layered compounds[51]. However it is clear that the main O-K lineshape change here stems from the TM valence change, and interesting pre-edge features also depend strongly on the hybridization character and the overall system covalency that often vary with electrochemical potentials. We therefore only clarify the TM redox in the NMC532 system in this work, and note that further efforts beyond sXAS will be necessary to address the possible evolution of oxygen states in this system.

Conclusions

In conclusion, we performed sXAS studies of the Ni, Mn, Co *L*-edges and O *K*-edge of NMC532 electrodes during the charging processes up to 4.5 V. We found the existence of about 20% Ni^{4+} in as-synthesized NMC532 along with roughly 60% Ni^{2+} and 20% Ni^{3+}, while Mn and Co are in the 4+ and 3+ oxidation states, respectively. The observed Ni^{4+} in NMC532 is likely associated with the incorporation of excess Li in the TM layer. The experimental charge capacity of NMC532 obtained at 4.2 V is related to oxidation of both Ni and Co. Only further oxidation of the Co cations is observed above 4.2 V. Unlike the well-defined Ni^{2+}, Ni^{3+} and Ni^{4+} ions, the Co in the charged electrodes shows intermediate valence states throughout the charge process. This

suggests that the Co promotes an itinerant electron system in NMC532, which plays an important role in improving the rate capability through Co doping. Mn^{4+} remains intact throughout the whole electrochemical process. Moreover, about 20% of Ni^{2+} is observed on the electrode surface at 4.5 V, which indicates that the electrode surface has either gone through surface reconstruction or reacted with the electrolyte at high voltage. This work demonstrates the power of sXAS for clarifying the evolution of the valence state and electronic structure of 3*d* transition-metal based battery electrodes.

Corresponding Author

*wlyang@lbl.gov (W. Y.). * lbliujun@gmail.com (J. L.)

ACKNOWLEDGMENT

The Advanced Light Source is supported by the Director, Office of Science, Office of Basic Energy Sciences, of the U.S. Department of Energy under Contract No. DE-AC02-05CH11231. This work was supported partially by the MRSEC Program of the National Science Foundation under Award Number DMR-1420073.

REFERENCES

[1] J.M. Tarascon, M. Armand, Nature, 414 (2001) 359-367.
[2] J.B. Goodenough, K.-S. Park, J. Am. Chem. Soc., 135 (2013) 1167-1176.
[3] B.L. Ellis, K.T. Lee, L.F. Nazar, Chem. Mater., 22 (2010) 691-714.
[4] J.B. Goodenough, Y. Kim, Chem. Mater., 22 (2009) 587-603.
[5] W.-S. Yoon, M. Balasubramanian, K.Y. Chung, X.-Q. Yang, J. McBreen, C.P. Grey, D.A. Fischer, J. Am. Chem. Soc., 127 (2005) 17479-17487.
[6] Y.-M. Lee, K.-M. Nam, E.-H. Hwang, Y.-G. Kwon, D.-H. Kang, S.-S. Kim, S.-W. Song, J. Phys. Chem. C, 118 (2014) 10631-10639.
[7] K.-W. Nam, S.-M. Bak, E. Hu, X. Yu, Y. Zhou, X. Wang, L. Wu, Y. Zhu, K.-Y. Chung, X.-Q. Yang, Adv. Funct. Mater., 23 (2013) 1047-1063.
[8] T. Kim, S. Bohang, N. Baimpas, C. Mocuta, Lecture Notes in Engineering and Computer Science, (2013).

[9] Y.-J. Gu, Y.-B. Chen, H.-Q. Liu, Y.-M. Wang, C.-L. Wang, H.-K. Wu, J. Alloys Compd., 509 (2011) 7915-7921.
[10] Y. Su, S. Cui, Z. Zhuo, W. Yang, X. Wang, F. Pan, ACS Applied Materials & Interfaces, 7 (2015) 25105-25112.
[11] T. Nagaura, K. Tozawa, Progress in Batteries & Solar Cells, 9 (1990) 209.
[12] S.-M. Bak, E. Hu, Y. Zhou, X. Yu, S.D. Senanayake, S.-J. Cho, K.-B. Kim, K.Y. Chung, X.-Q. Yang, K.-W. Nam, ACS Applied Materials & Interfaces, 6 (2014) 22594-22601.
[13] S.-K. Jung, H. Gwon, J. Hong, K.-Y. Park, D.-H. Seo, H. Kim, J. Hyun, W. Yang, K. Kang, Adv. Energy Mater., 4 (2014) 1300787-n/a.
[14] S. Hwang, S.M. Kim, S.-M. Bak, K.Y. Chung, W. Chang, Chem. Mater., 27 (2015) 6044-6052.
[15] D. Mohanty, A.S. Sefat, E.A. Payzant, J. Li, D.L. Wood Iii, C. Daniel, J. Power Sources, 283 (2015) 423-428.
[16] J.F. Moulder, W.F. Stickle, P.E. Sobol, K.D. Bomben, Handbook of X-ray Photoelectron Spectroscopy, Physical Electronics, Inc., 1992.
[17] M.C. Sánchez, J. García, J. Blasco, G. Subías, J. Perez-Cacho, Phys. Rev. B, 65 (2002) 144409.
[18] D.Y.W. Yu, K. Yanagida, Y. Kato, H. Nakamura, J. Electrochem. Soc., 156 (2009) A417-A424.
[19] N. Yabuuchi, K. Yoshii, S.-T. Myung, I. Nakai, S. Komaba, J. Am. Chem. Soc., 133 (2011) 4404-4419.
[20] A.Y. Ignatov, N. Ali, S. Khalid, Phys. Rev. B, 64 (2001) 014413.
[21] J.-M. Kim, H.-T. Chung, Electrochim. Acta, 49 (2004) 937-944.
[22] S.P. Cramer, F.M.F. DeGroot, Y. Ma, C.T. Chen, F. Sette, C.A. Kipke, D.M. Eichhorn, M.K. Chan, W.H. Armstrong, J. Am. Chem. Soc., 113 (1991) 7937-7940.
[23] B. Gilbert, B.H. Frazer, A. Belz, P.G. Conrad, K.H. Nealson, D. Haskel, J.C. Lang, G. Srajer, G. De Stasio, The Journal of Physical Chemistry A, 107 (2003) 2839-2847.
[24] W.-S. Yoon, K.-Y. Chung, K.-H. Oh, K.-B. Kim, J. Power Sources, 119–121 (2003) 706-709.
[25] L. Qinghao, Q. Ruimin, L.A. Wray, C. Jun, Z. Zengqing, C. Yanxue, Y. Shishen, P. Feng, H. Zahid, Y. Wanli, J. Phys. D: Appl. Phys., 49 (2016) 413003.
[26] R.M. Qiao, L.A. Wray, J.H. Kim, N.P.W. Pieczonka, S.J. Harris, W.L. Yang, J. Phys. Chem. C, 119 (2015) 27228-27233.
[27] R. Qiao, Y. Wang, P. Olalde-Velasco, H. Li, Y.-S. Hu, W. Yang, J. Power Sources, 273 (2015) 1120-1126.
[28] R. Qiao, K. Dai, J. Mao, T.-C. Weng, D. Sokaras, D. Nordlund, X. Song, V.S. Battaglia, Z. Hussain, G. Liu, W. Yang, Nano Energy, 16 (2015) 186-195.
[29] W. Yang, X. Liu, R. Qiao, P. Olalde-Velasco, J.D. Spear, L. Roseguo, J.X. Pepper, Y.-d. Chuang, J.D. Denlinger, Z. Hussain, Journal of Electron Spectroscopy and Related Phenomena, 190 (2013) 64-74.
[30] R.M. Qiao, I.T. Lucas, A. Karim, J. Syzdek, X.S. Liu, W. Chen, K. Persson, R. Kostecki, W.L. Yang, Adv. Mater. Interfaces, 1 (2014) 1300115-1300120.
[31] M. Matsubara, T. Uozumi, A. Kotani, J. Claude Parlebas, J. Phys. Soc. Jpn., 74 (2005) 2052-2060.
[32] C. Piamonteze, F.M.F. de Groot, H.C.N. Tolentino, A.Y. Ramos, N.E. Massa, J.A. Alonso, M.J. Martínez-Lope, Phys. Rev. B, 71 (2005) 020406-020409.

[33] S. Yang, X. Wang, X. Yang, Z. Liu, Q. Wei, H. Shu, International Journal of Electrochemistry, 2012 (2012) 9.
[34] J. Wang, Y. Yu, B. Li, T. Fu, D. Xie, J. Cai, J. Zhao, Phys. Chem. Chem. Phys., 17 (2015) 32033-32043.
[35] J. Zaanen, G.A. Sawatzky, Phys. Rev. B, 33 (1986) 8074-8083.
[36] F.M.F. de Groot, J.C. Fuggle, B.T. Thole, G.A. Sawatzky, Phys. Rev. B, 42 (1990) 5459-5468.
[37] X. Liu, J. Liu, R. Qiao, Y. Yu, H. Li, L. Suo, Y.-s. Hu, Y.-D. Chuang, G. Shu, F. Chou, T.-C. Weng, D. Nordlund, D. Sokaras, Y.J. Wang, H. Lin, B. Barbiellini, A. Bansil, X. Song, Z. Liu, S. Yan, G. Liu, S. Qiao, T.J. Richardson, D. Prendergast, Z. Hussain, F.M.F. de Groot, W. Yang, J. Am. Chem. Soc., 134 (2012) 13708-13715.
[38] R. Qiao, K. Dai, J. Mao, T.-C. Weng, D. Sokaras, D. Nordlund, X. Song, V.S. Battaglia, Z. Hussain, G. Liu, W. Yang, Nano Energy, 16 (2015) 186-195.
[39] F. de Groot, A. Kotani, Core Level Spectroscopy of Solids, CRC Press Taylor & Francis Group, Boca Raton, FL, USA, 2008.
[40] J.-H. Kim, N.P.W. Pieczonka, P. Lu, Z. Liu, R. Qiao, W. Yang, M.M. Tessema, Y.-K. Sun, B.R. Powell, Adv. Mater. Interfaces, 2 (2015) 1500109-1500121.
[41] T. Mizokawa, Y. Wakisaka, T. Sudayama, C. Iwai, K. Miyoshi, J. Takeuchi, H. Wadati, D.G. Hawthorn, T.Z. Regier, G.A. Sawatzky, Phys. Rev. Lett., 111 (2013) 056404.
[42] J.-H. Kim, N.P.W. Pieczonka, Z. Li, Y. Wu, S. Harris, B.R. Powell, Electrochim. Acta, 90 (2013) 556-562.
[43] D.H. Jang, Y.J. Shin, S.M. Oh, J. Electrochem. Soc., 143 (1996) 2204-2211.
[44] F. Lin, I.M. Markus, D. Nordlund, T.-C. Weng, M.D. Asta, H.L. Xin, M.M. Doeff, Nat. Commun., 5 (2014) 3529.
[45] M. Lin, L. Ben, Y. Sun, H. Wang, Z. Yang, L. Gu, X. Yu, X.-Q. Yang, H. Zhao, R. Yu, M. Armand, X. Huang, Chem. Mater., 27 (2015) 292-303.
[46] X. Liu, D. Wang, G. Liu, V. Srinivasan, Z. Liu, Z. Hussain, W. Yang, Nat. Commun., 4 (2013) 2568.
[47] F.M.F. de Groot, M. Grioni, J.C. Fuggle, J. Ghijsen, G.A. Sawatzky, H. Petersen, Phys. Rev. B, 40 (1989) 5715-5723.
[48] D.-H. Seo, J. Lee, A. Urban, R. Malik, S. Kang, G. Ceder, Nat Chem, 8 (2016) 692-697.
[49] K. Luo, M.R. Roberts, R. Hao, N. Guerrini, D.M. Pickup, Y.-S. Liu, K. Edström, J. Guo, A.V. Chadwick, L.C. Duda, P.G. Bruce, Nat Chem, (2016).
[50] M. Sathiya, G. Rousse, K. Ramesha, C.P. Laisa, H. Vezin, M.T. Sougrati, M.L. Doublet, D. Foix, D. Gonbeau, W. Walker, A.S. Prakash, M. Ben Hassine, L. Dupont, J.M. Tarascon, Nat. Mater., 12 (2013) 827-835.
[51] M. Oishi, C. Yogi, I. Watanabe, T. Ohta, Y. Orikasa, Y. Uchimoto, Z. Ogumi, J Power Sources, 276 (2015) 89-94.

SUPPLEMENTARY:

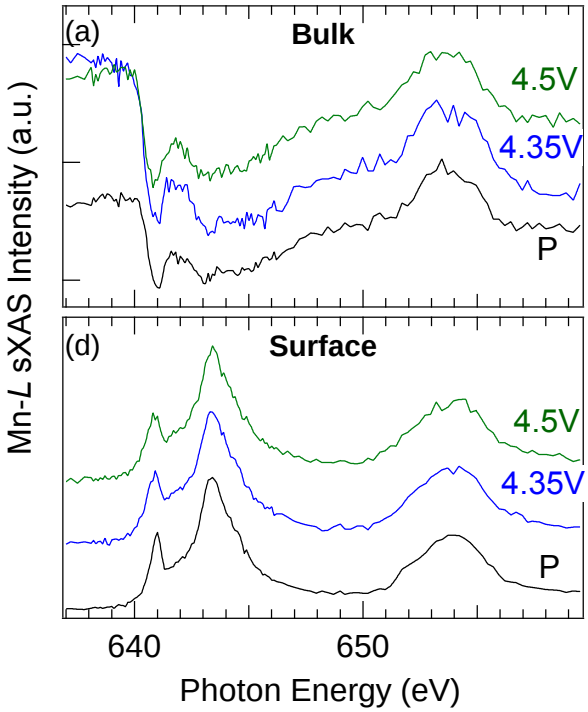

Figure S1: Mn-*L* sXAS spectra of NMC532 at different voltages. (a) bulk-sensitive TFY. (b) surface-sensitive TEY.

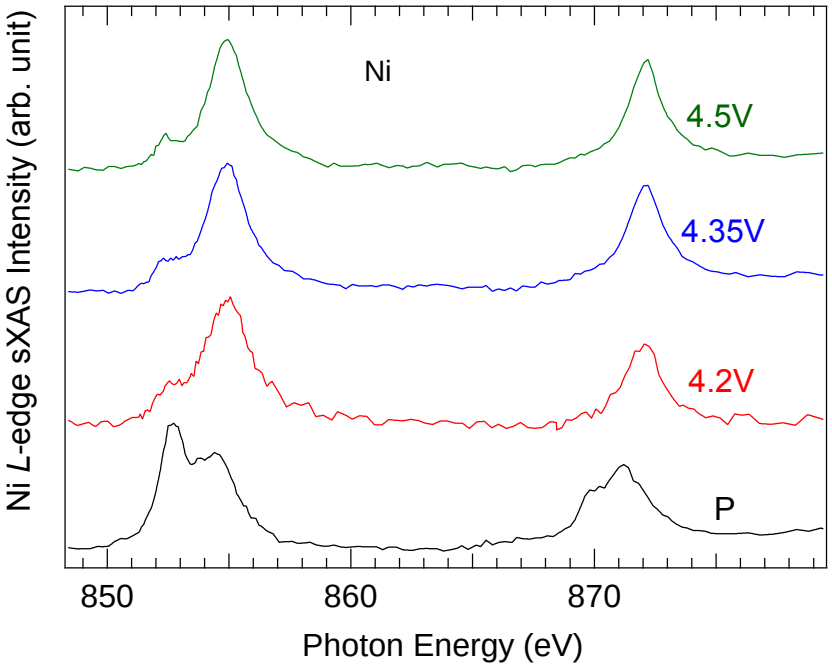

Figure S2: Evolution of bulk-sensitive Ni-*L* TFY sXAS spectra at different voltage.

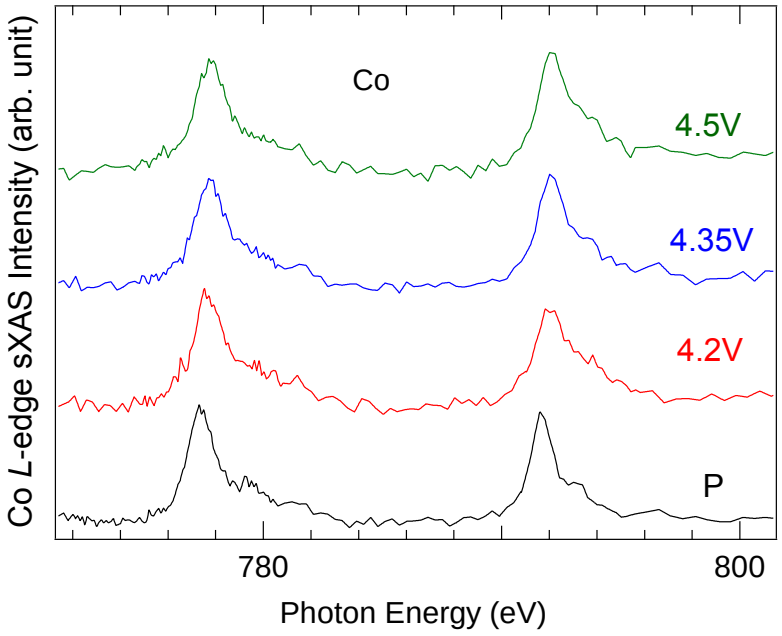

Figure S3: Evolution of bulk-sensitive Co-*L* TFY sXAS spectra at different voltage.